Sayed Tabatabaei et al., *BioImpacts.* 2025;15:27558
doi: 10.34172/bi.2023.27558
https://bi.tbzmed.ac.ir/

Optimized cutaneous delivery of anti-wrinkle dipeptide KT via molecular modification: Preformulation, permeation, and the importance of conjugate chain length

Mahsa Sayed Tabatabaei[1], Farzad Kobarfard[2], Reza Aboofazeli[1,3], Sorour Ramezanpour[4], Hamid Reza Moghimi[1,3*]

[1]Department of Pharmaceutics and Pharmaceutical Nanotechnology, School of Pharmacy, Shahid Beheshti University of Medical Sciences, Tehran, Iran
[2]Department of Medicinal Chemistry, School of Pharmacy, Shahid Beheshti University of Medical Sciences, Tehran, Iran
[3]Protein Technology Research Center, Shahid Beheshti University of Medical Sciences, Tehran, Iran
[4]Peptide Chemistry Research Center, K. N. Toosi University of Technology, Tehran, Iran

Article Info

Article Type:
Original Article

Article History:
Received: 10 Aug. 2022
Revised: 27 Sep. 2022
Accepted: 28 Sep. 2022
ePublished: 18 Jul. 2023

Keywords:
Dipeptide KT
Pal-KT
Anti-wrinkle peptide
Molecular modification
Fatty acid conjugation
Skin permeation

Abstract

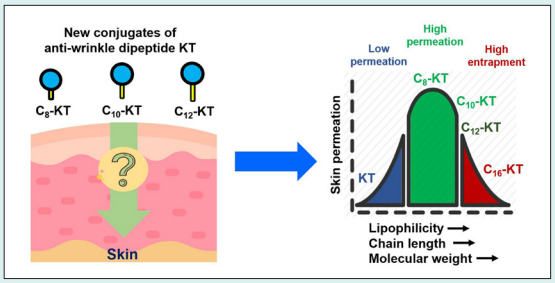

Introduction: Anti-aging peptides, such as dipeptide KT, are promising rejuvenating agents and have recently received significant attention. However, their hydrophilic nature makes skin absorption therapeutically inadequate. The excessive hydrophilicity of peptides is partially solved by lipoidal conjugates, however, the increased molecular weight due to conjugation creates a new obstacle to skin permeation.

Methods: In an attempt to concurrently solve these limitations, here we have studied different short-mid chain fatty acids (C_6-C_{18}) conjugates of dipeptide KT. Different fatty acid chain lengths of C_6, C_8, C_{10}, C_{12}, C_{14}, C_{16}, and C_{18} were considered to be conjugated with KT and screened *in-silico*. Of those, C_8, C_{10}, and C_{12} were preferred and synthesized alongside two controls of the parent drug (KT) and C_{16} (Pal-KT) as the commercialized form to be studied mechanistically. Subsequently, they were structurally characterized and underwent preformulation, supramolecular investigations (e.g., thermal behavior, solubility, surface-acting, crystalline structure), and skin absorption studies.

Results: Data showed that the synthesized conjugates substantially outperformed Pal-KT in terms of molecular weight, lipophilicity, melting point, and aqueous solubility. In addition, unlike KT, they all demonstrated amphiphilicity-related features. The maximum and minimum skin permeation were assigned to C_8-KT (33.2%) and KT (0.004%). Moreover, permeability coefficients (Kp) of the C_8-KT, C_{10}-KT, C_{12}-KT, and C_{16}-KT were calculated to be about 22000, 3800, 3400, and 1600 times higher than KT, respectively.

Conclusion: Conjugating lower molecular weight fatty acids and optimizing lipophilicity can enhance molecular properties, skin absorption, and the ability to form supramolecular structures. This, in turn, leads to the development of superior anti-wrinkle products and formulations.

Introduction

Aging is a complicated biological phenomenon, whose effect appears on the skin more than any other organ.[1] The unpleasant appearance of wrinkled skin could negatively affect psychosocial health.[2] So, anti-aging strategies have recently garnered attention. Cosmeceutical peptides are pioneer representatives of anti-aging components. Despite the desired benefits, their hydrophilic nature hinders their permeation through the lipophilic stratum corneum in therapeutic amounts.[3,4]

There are various strategies to enhance transdermal delivery of hydrophilic compounds like using chemical enhancers,[5,6] physical enhancers,[7] non-covalent complexation to lipophilic compounds,[8] encapsulation within the nanocarriers, and improving their lipophilicity by chemical modification through conjugation with

*Corresponding author: Hamid Reza Moghimi, Email: hrmoghimi@sbmu.ac.ir and hrmoghimi@yahoo.com

lipophilic molecules,[9-11] also known as peptide lipidation.[12] The latter, as a straightforward strategy, is the subject of the present investigation.

The conjugation strategy commonly uses fatty acid conjugation, specifically palmitoylation. Palmitoylation involves the conjugation of a palmitic acid (abbreviated as Pal) with a 16-carbon backbone to the N-terminal of amino acids through a peptide bond. This process is highly relevant for modifying the physicochemical properties of cosmetic oligopeptides.[13] Besides the improvement of skin absorption by improving lipophilicity, palmitoylation plays an important role in the half-life and stability improvement of the peptides.[12] Unfortunately, such kind of modifications increases the molecular weight of the penetrant and, therefore, creates a new obstacle in permeation through the skin, as described below for KTTKS.

Pentapeptide KTTKS (lysine-threonine-threonine-lysine-serine), a fragment of procollagen I, is an efficient collagenesis stimulating signal pentapeptide, the use of the intact form of which is restricted due to its high hydrophilicity and low skin permeability. Pal-KTTKS is its more lipophilic and commonly used analog whose collagen production effectiveness has been previously proven.[14] Although Pal-KTTKS shows an improved logP compared to KTTKS (from 3.54- to 3.72), the increased molecular weight (from 564 to802 Da) causes a new problem for skin permeation.[15] In our previous investigations, we tried to solve this problem using small terpene penetration enhancers as the conjugates. Our results revealed that smaller conjugates (e.g., citronellic acid-KTTKS) can improve permeation of KTTKS in comparison to its Pal-derivatives.[16]

Another possible approach is to use smaller peptides with high potencies, such as dipeptide KT (lysine-threonine). However, KT also faces the challenge of being hydrophilic. Fortunately, Pal-KT, which is a commercialized and stable form of KT, has partially overcome this obstacle.[17,18] However, it is a poorly water-soluble compound, and considering the molecular weight hindrance, as discussed above, it is expected to achieve more efficient lipoidal conjugates through using smaller and more hydrophilic moieties, the subject of the present investigation.

Lipoidal peptide conjugates may also self-assemble due to their amphiphilic nature. If so, they may be formulated as self-delivery (or carrier-free) systems. In the self-delivery systems, the drug molecule undertakes the structural and functional roles concurrently (i.e., as an active pharmaceutical ingredient and a main structural unit). So, the carrier-mediated limitations and auxiliary role of excipients are circumvented.[19] Besides, it has been recently reported that self-assembled structures of a lipoidal dipeptide (Pal-glycine-histidine) act as a permeation enhancer for transdermal drug delivery.[20]

The current study aims to improve skin absorption of KT via lipoidal conjugation. So, here, a range of lipoidal derivatives of KT with relatively short chain length fatty acids, was firstly synthesized and structurally characterized to obtain peptides with adjusted polarity, while maintaining the molecular weight in the appropriate range. Then, the resultant conjugates underwent preformulation studies as well as skin absorption to determine if they could serve as promising alternatives to Pal-KT in the future. Also, the self-assembly capability of lipoidal conjugates in the aqueous media was investigated. This is important because self-assembled supramolecular structures not only allow self-delivery of drug molecules (i.e., with no need for the additional carrier) but may also act as skin permeation enhancers. This hypothesis, investigating whether self-assembled structures can enhance skin absorption of conjugates, is being explored by the same research team as the second part of this project.

Materials and Methods

Materials

Protected amino acids, Fmoc-Thr(tBu)-OH and Fmoc-Lys(Boc)-OH, 2-CTC (2-chlorotrityl chloride) resin, and TBTU (*O*-(Benzotriazole-1-yl)-*N*,*N*,*N*′,*N*′-tetramethyluronium tetrafluoroborate), were purchased from GL Biochem (Shanghai, China). All fatty acids including caprylic acid, capric acid, lauric acid, and palmitic acid (with an 8-, 10-, 12-, and 16-carbon atom chain, respectively), DCM (dichloromethane), methanol, DMF (*N*,*N*-dimethylformamide), diethyl ether, DIEA (*N*,*N*-diisopropylethylamine), KCN (potassium cyanide), TIS (triisopropylsilane), and ACN (acetonitrile) were obtained from Merck (Darmstadt, Germany). TFA (trifluoroacetic acid) and piperidine were both purchased from Exir GmbH, respectively through branches in Wien (Austria) and Munich (Germany). Ninhydrin (2,2-dihydroxyindane-1,3-dione) was obtained from BDH Chemicals (Dorset, UK). DMSO (dimethyl sulfoxide) and ethanol 96% were purchased from Chem Lab (Zedelgem, Belgium) and Pars Alcohol (Tehran, Iran), respectively.

Skin samples

Full-skin rat abdominal skin samples were used for permeation studies. Around 8-weeks old healthy adult male Sprague-Dawley rats (weighing 220-250 g) were supplied from the Pasteur Institute of Iran (Tehran, Iran). Through a painless technique for humane euthanasia of laboratory animals, the rats were anesthetized with a stress-free quick-acting anesthetic agent, isoflurane (Merck, Germany), before being sacrificed. Subsequently, the full-thickness abdominal skin pieces were excised and thoroughly shaved by an electrical hair clipper (Moser, Germany). They were removed from adherent fat and subcutaneous tissue and circular pieces of skin with appropriate diameter were obtained by cutting, which then was wrapped in an aluminum foil and frizzed at -20 °C until use.

Selection of fatty acids

Molecular weight and shape affect percutaneous permeation and are important in the selection of ligands. As straight-chain derivatives are more fortunate to pass the skin than the branched ones[21] and also as the commercialized conjugate of KT contains a linear fatty acid (palmitic acid), a range of linear fatty acids with different chain lengths (6-18 carbons) was selected for binding to KT here. Conjugations of KT with caproic acid (C_6-KT), caprylic acid (C_8-KT), capric acid (C_{10}-KT), lauric acid (C_{12}-KT), myristic acid (C_{14}-KT), palmitic acid (C_{16}-KT), and stearic acid (C_{18}-KT) were considered as the initial candidates to be evaluated. Octanol/water partition coefficient (logP) was predicted for KT and its amphiphilic derivatives using ACD/ChemSketch version 12.0 freeware software (Advanced Chemistry Development, Canada). Also, skin permeability was calculated as previously stated in the Potts and Guy equation according to Eq.1,

$$\log Kp\ (\mathrm{cm/s}) = 0.71 - 0.0061MW - 6.3 \qquad \text{(Eq.1)}$$

where Kp and MW stand for skin permeability coefficient and molecular weight, respectively.[22] Considering these parameters the most suitable candidates were screened for further studies.

Synthesis and lyophilization

KT and its conjugates (C_8-KT, C_{10}-KT, C_{12}-KT, and C_{16}-KT) were manually synthesized using the standard Fmoc solid-phase peptide synthesis (SPPS) method (Fig. 1A) on the 2-CTC resin (5 g). A stepwise elongation protocol with a 2-fold excess of each protected amino acid derivatives was employed. The deprotection process was accomplished by 25% (v/v) piperidine in DMF for 10 min before each coupling. DMF solution containing TBTU (4.81 equiv.) and DIEA (5 equiv.) were used to activate the Fmoc amino acids. The loaded resin shrank using DCM (50 mL) and methanol (50 mL), followed by drying under a vacuum. After weighing and splitting into five equal portions, one part was separated to be cleaved and form KT. The remnant mass underwent Fmoc-deprotection, followed by respective fatty acids coupling (3-fold excess) to the N-terminus of the resin-bound peptide under the same conditions listed. For cleavage and final deprotection, we used a cocktail of TFA (10 mL), TIS (380 µL), methanol (250 µL), and water (250 µL) for 1 g resin-conjugate. After TFA evaporation, the obtained mixtures were precipitated in diethyl ether, followed by centrifugation (5702, Eppendorf, Germany) at 5000 g for 15 minutes. Then, the precipitants were re-dispersed in deionized water, frozen at -70 °C for 24 hours, and lyophilized using a freeze dryer (ALPHA1-2D, Martin Christ, Germany) for 48h under the pressure of 0.4 bar.

Purity determination

The purity of peptides was determined using a reverse-phase high-performance liquid chromatography (RP-HPLC) method with UV absorption at 220 nm. Briefly, a Boston Green ODS-AQ C18 column (250 mm × 4.6 mm, 5 µm) was used under AB gradient mode at a flow rate of 1.0 mL/min and ambient temperature. The eluent A and B were 0.1% v/v TFA in water and acetonitrile, respectively.[23] The purity percentage was calculated as the ratio of the desired product to the impure sample.

Electrospray ionization mass spectroscopy (ESI-MS)

The products were identified by ESI-MS (6410 Series Triple Quad LC/MS, Agilent, USA). In brief, we prepared and injected aqueous solutions containing trace amounts

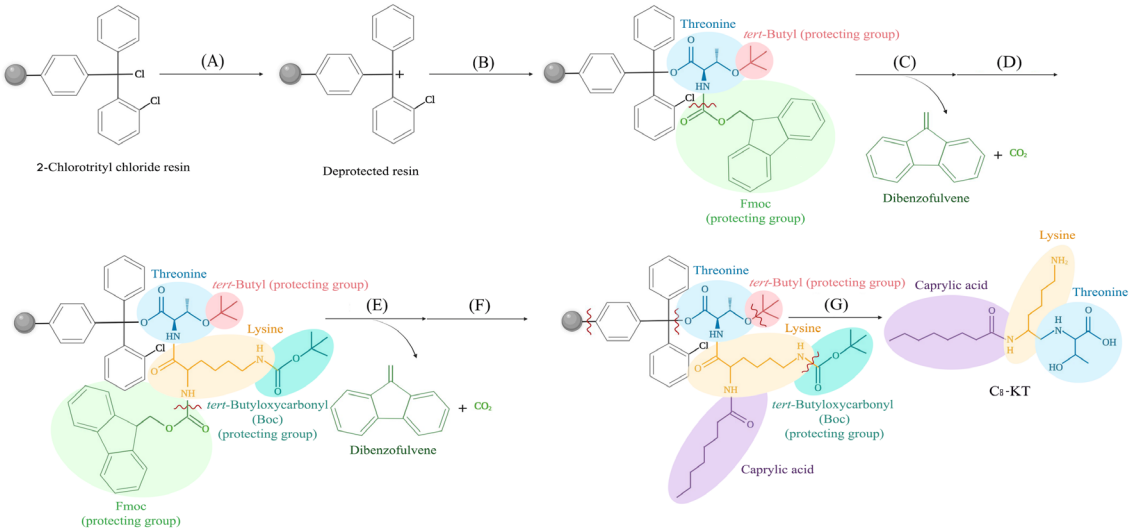

Fig. 1. A schematic representation of the synthesis procedure used in the present work (here the synthesis process of C8-KT is shown; other conjugates were also synthesized similarly); (A) transient deprotection of 2-chlorotrityl chloride resin, (B) coupling the first protected amino acid, threonine, (C) deprotection (Fluorenylmethyloxycarbonyl, Fmoc, removal) of threonine, (D) coupling the second protected amino acid, lysine, (E) deprotection (Fmoc removal) of lysine, (F) coupling the fatty acid (caprylic acid), and (G) cleavage of the peptide from the resin and final deprotection.

of each synthesized compound. Observation of the hydrogen adducts equivalent to the calculated molecular weight ($(M+H)^+$) or its multiplied (e.g., $(2M+H)^+$) was considered an indication of the successful synthesis.

Fourier transform infrared (FT-IR) spectroscopy

Spectra were recorded using a professional FT-IR spectrometer (WQF-510, Rayleigh Optics, China) equipped with a Potassium bromide KBr beamsplitter and a DTGS detector. Lyophilized powders were physically mixed with KBr and pelleted with a compression force of 40 MPa, followed by being scanned 100 times over the wavelength range of 4000-400 cm^{-1}. The transmittance spectra were plotted as a function of wavenumber (cm^{-1}). The insights provided by FT-IR patterns were used to verify the chemical structure of synthesized compounds.

Thermogravimetric Analysis (TGA)

Using a thermogravimetric analyzer (TGA-50, Shimadzu, Japan), the weight loss of peptides (an indication of water loss and the possibility of thermal instability) was monitored over the range of 25-600 °C at the heating rate of 10 °C/min.

Melting point and differential scanning calorimetry (DSC)

The capillary method was employed to measure the melting points of peptides. The capillary tubes containing packed samples were placed in the melting point apparatus (IA9000 Series Melting Point Apparatus, Electrothermal, Germany). The temperature increased with the ramp rate of 5 °C/min, and immediately after the whole sample melted, the temperature was recorded.

DCS (DSC-60, Shimadzu, Japan) was employed to determine the heat flow and thermal transitions of peptide conjugates. After calibration with indium as the standard, an approximate amount of 5 mg for each sample was placed in an aluminum pan and sealed. In the case of KT and C_8-KT, due to their gel-like state, pressure-proof pans were employed. Under nitrogen purging and with a heating rate of 10 °C/min, the samples were scanned from room temperature to 300 °C.

X-ray diffraction (XRD)

To determine the crystallinity, dry samples of peptides were analyzed by an X-ray diffractometer (X'Pert PRO MPD, PANalytical BV, The Netherlands) at 25.0 °C, using Cu Kα1 (40 kV, 40 mA, λ=1.54056 Å) radiation. Over the 2θ range of 2-80°, data were acquired with a step size of 0.026° and nominal time per step of 0.1 s. Fixed divergence and anti-scatter slits of 1.0° were used together with a beam mask of 10 mm. All scans were carried out in the continuous mode. Peak positions, the corresponding repeat distances, and relative intensities were obtained using the software PANalytical X'pert HighScore version 3.0.5. (Malvern Panalytical, UK).

Prediction of solubility

LogS (aqueous solubility in mol/L) of KT and its derivatives were predicted using ALOGPS 2.1 software,[24] wherein the calculations are performed based on the chemical structure in the input format 'SMILES' (simplified molecular-input line-entry system).

Polarized light microscopy

Texture and birefringence of samples were examined using a polarizing optical microscope (Ceti Magnum-POL Trinocular Compound Polarization Microscope, Medline Scientific, UK) equipped with a microscope camera (DFK MKU130, The Imaging Source, Germany). In general, birefringence is observed in all crystalline structures except cubic crystals. At laboratory temperature, glass slides of the samples were prepared and observed under cross-polarized light with a magnification of 40x. The images were recorded using IC capture free software version 2.4. (The Imaging Source, Germany).

Field emission scanning electron microscopy (FE-SEM)

The morphology and topography of peptides were also investigated using an FE-SEM (MiRa3, TESCAN, Czech Republic) at a voltage of 15.0 kV. Dry samples were settled on the glass grids which were then coated with platinum; afterward, they were allowed to completely dry overnight at room temperature before the examination.

Determination of surface tension and critical micelle concentration (CMC)

To investigate whether amphiphilic KT derivatives show surfactant-like behavior, the process of lowering the surface tension of water by the lipoidal conjugates as well as their surface tension values at the static zone (i.e., minimum surface tension beyond CMC where is no longer affected by concentration) were compared with the surface tension value of deionized water. Aqueous solutions of KT and its conjugates with the initial concentration of twice the predicted solubility were freshly prepared.[25] Surface tension and CMC of all samples were measured using the Du Noüy ring method at 25±0.5 °C employing a force tensiometer (K100, KRÜSS GmbH, Germany). For each test, 120 ml of sample solution was poured into a clean beaker. The platinum ring was completely immersed in the solution, after which it was slowly lifted from the liquid surface. At the point where the ring was completely detached, the force was recorded and related to the surface tension using ADVANCE software version 1.7 (KRÜSS software, Germany). To ensure accuracy and reproducibility, the measurements were performed in triplicate.

Particle size by dynamic light scattering (DLS)

To evaluate whether the synthesized conjugates may show self-assembling capability (in the aqueous medium and ambient temperature), 1 mL of each sample (at the

concentration of two-folds of the predicted solubility to ensure particle formation) was poured into a glass cuvette and the particle size distribution was measured by DLS using a Malvern Zetasizer Nano ZS instrument (Malvern Instruments Ltd., Worcestershire, UK). All DLS measurements were performed at 173° backscatter angle, for 3 cycles, and at 25°C with an equilibration time of 120 seconds. The intensity-based Z-average data (on 13 scans) was relied upon to obtain hydrodynamic diameters.

Peptide assay by flow injection analysis (FIA)

Detection and quantification of KT and its conjugates were performed using a mass spectrometer (6410 Series Triple Quad LC/MS, Agilent, USA) equipped with an ESI source in flow injection analysis (FIA) mode. Being taken from the autosampler, samples were injected into the mass spectrometer and analyzed by direct infusion.

Short-term stability studies

Aqueous solutions of KT and its conjugates were prepared with specified concentrations, followed by incubation at four different temperatures (−20, 4, 25, and 37 °C) for 72 hours. Subsequently, according to the previously described FIA method, the samples were quantified and compared with the fresh samples containing the same initial concentrations.

Ex-vivo skin permeation studies

To investigate the absorption of drug candidates from rat skin, unjacketed upright Franz diffusion cells (Dorsa, Iran) with a surface area of 2.0 cm^2 were utilized. At the mating surface of the donor and receptor chamber, a full-thickness skin sample was mounted. Peptides at their saturated solubility concentrations (based on logS values) were used as donor phases and the receptor chambers were filled with 5 mL 10%(v/v) hydroethanolic solution to ensure the sink condition. The sampling/replacing port and the donor chamber input part were sealed with a laboratory wrapping film to avoid solvent evaporation. Then, the whole system was carefully placed in a water bath set at a controlled temperature of 37±0.5 °C, under a 300rpm constant stirring for 48h. Subsequently, 1 mL aliquots of receptor phase were sampled at 1, 2, 4, 6, 8, 24, and 48 hours, followed by immediate replacement by the same volume of fresh hydroethanolic solution. After collecting each sample, it was instantly transferred to the freezer to be stored at -20 °C until being analyzed by FIA, as described previously. After plotting the permeated drug as a function of time, the permeation flux and permeability coefficient of each compound were calculated and compared.

Statistical analysis

Data were analyzed using IBM SPSS Statistics version 24.0 software (IBM, Armonk, NY, USA). Independent sample *t* test analyses were used to determine whether the values were statistically different. The differences were considered significant at $P \leq 0.05$ and highly significant at $P \leq 0.001$.

Results

Conjugates design, synthesis, and purity

In silico predicted logP, Kp, and molecular weight of peptides are listed in Table 1. Based on the previous experiences, several requirements have been suggested for penetrants for optimal delivery through the skin by passive diffusion including molecular weight <500 Da,[26-28] logP values of 1-4,[29] and Kp>1.38×10^{-6} cm/s.[30] Accordingly, an optimal range for the length of the fatty acid chain can be defined in theory for the conjugates. As shown in Table 1, C_8-KT, C_{10}-KT, and C_{12}-KT are optimal in all respects. Thus, they were selected for synthesis and further investigation. Furthermore, C_{16}-KT (Pal-KT) as the most common and commercialized derivative, and KT as the oligopeptide base, were synthesized and studied. The successful synthesis of peptides was verified by mass spectroscopy, whereupon the observed values concurred well with corresponding calculated quantities.

The purity of peptides was qualitatively verified by ESI-mass spectra, which showed no significant additional peaks. The purity values were also determined quantitatively using RP-HPLC. The purity percentage for KT, C_8-KT, C_{10}-KT, C_{12}-KT, and C_{16}-KT were respectively calculated as 99.2, 96.6, 98.4, 98.8, and 95.6% (±0.2%). Regarding the satisfactory yield of at least 95% for all samples, no additional purification was required. The

Table 1. *In-silico* prediction of logP, permeability coefficient (Kp) values, molecular formulas and weights of KT and its conjugates (C_n-KT, n=6-18)

Compound	Molecular Formula	MW (Da)	Calculated logP	Estimated Kp (cm/s)
KT	$C_{10}H_{21}N_3O_4$	247.3	-2.00	9.82×10^{-5}
C_6-KT	$C_{16}H_{31}N_3O_5$	345.5	0.38	2.92×10^{-4}
C_8-KT	$C_{18}H_{35}N_3O_5$	373.5	1.44	5.23×10^{-4}
C_{10}-KT	$C_{20}H_{39}N_3O_5$	401.5	2.50	9.36×10^{-4}
C_{12}-KT	$C_{22}H_{43}N_3O_5$	429.6	3.57	1.68×10^{-3}
C_{14}-KT	$C_{24}H_{47}N_3O_5$	457.6	4.63	3.02×10^{-3}
C_{16}-KT	$C_{26}H_{51}N_3O_5$	485.7	5.69	5.39×10^{-3}
C_{18}-KT	$C_{28}H_{55}N_3O_5$	512.7	6.75	9.71×10^{-3}

molecular structure of KT conjugates is illustrated in Fig. 2A.

Confirmation of chemical structure

The chemical identities of KT and its related conjugates were established using FT-IR analysis (Fig. 2B). FT-IR spectra of the lipoidal conjugates of KT showed strong peaks at wavenumbers 2850-3000 cm^{-1}, assigned to C-H groups in the fatty acid chains; the longer the chain length the greater intensity. Moderate peaks in all samples, at 3100-3500 cm^{-1}, were allocated to N-H stretching absorption. The strong broad peaks at wavenumbers 2400-3400 cm^{-1} are representative of carboxylic acid functional groups of threonine. In the case of dipeptide KT, due to being smaller than other structures, O-H is the dominant peak and masks the peak of the N-H functional group. In all spectra, there are strong peaks at 1630-1770 cm^{-1} and relatively high-intensity peaks at 1520-1630 cm^{-1}, which are assigned to C=O functional groups (amide, acid, and aldehyde) and N-H bending vibrations, respectively. Moreover, there are medium peaks at wavenumbers 1460-1490 cm^{-1} and weak peaks at 1330-1400 cm^{-1}, representing CH_2 and CH_3 bending vibrations, respectively. The weaker peaks at 1000-1250 cm^{-1} are representatives of the C-N functional group in the threonine-lysine structure, which is in common in the whole samples. Collectively, the FT-IR spectra of all samples follow the same pattern, and the functional groups identified correspond well with the intended structures; which logically confirms the correctness of synthesized structures.

Thermal behavior

TGA thermograms of KT and its lipoidal conjugates are shown in Fig. 3A. Data shows that there is no weight loss over 20 to130-140 °C (region I). This initial phase is then followed by relatively similar multi-stage weight loss phases (regions II to V). As KT and its derivatives are not expected to be volatile, the weight loss can be attributed to the decomposition process, which occurs following the evaporation and decomposition of products (into H_2O and CO_2, for instance). In decomposition phases, generally, the higher the molecular weight (lipophilicity in our case), the lower the slope. Additionally, the percentage of weight loss in the first decomposition phase (region II), is inversely related to lipophilicity. Despite the slight differences, there is the same thermal behavior pattern followed by them all. Our experiment is in agreement with previous findings on the direct correlation of chain length with thermal stability.[31]

In capillary melting point studies, C_{10}-KT, C_{12}-KT, and C_{16}-KT showed distinct melting points at 131.7, 132.5, and 136.7 °C, respectively (Data are mean ± 0.1 °C). KT and C_8-KT, on the other hand, did not exhibit melting but exhibited a color change at approximately 140.0 °C and

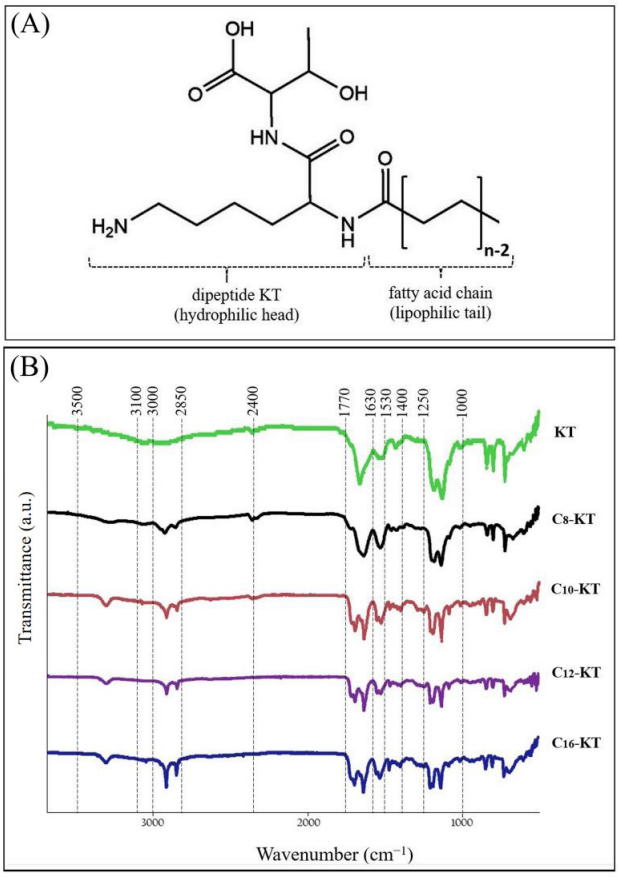

Fig. 2. (A) General structure formula and (B) Comparative FT-IR spectra of KT and its lipoidal conjugates (Cn-KT, n=6-18).

131.9 ºC, respectively, indicating possible decomposition.

According to the DSC thermograms (Fig. 3B), the longer-chain conjugates of KT (C_{10}-KT, C_{12}-KT, and C_{16}-KT) showed one high-intensity endothermic transitions at 131.7, 132.7, and 138.0 ºC, respectively (with the enthalpy change, ΔH, between 78.3 and 88.1 J/g) which are in good agreement with the capillary melting point results (P>0.05). In general, in the homologous series, the longer the hydrocarbon chain, the higher the melting point.[32] This increasing trend holds for C_{10}-KT, C_{12}-KT, and C_{16}-KT. Needless to say, this rule applies to chains whose carbon difference is a multiple of 2. In the case of the KT and C_8-KT (Fig. 3B), the peaks observed at about 140 and 130 ºC, respectively, can be probably attributed to decomposition, taking into account the observations during the melting point test. As will be explained in the next section, C_8-KT has a crystalline structure while KT is amorphous. So, the endothermic peak that appeared at about 90 ºC in the DSC thermograms of C_8-KT is likely to indicate the physical or mesophase transitions due to the internal structural changes. For KT, the endothermic peak at around 54 ºC could be possibly attributed to the glass transition (considering the amorphous nature of KT) or phase transition (since it has been previously reported for amorphous di-phenylalanine peptide).[33] However, a definitive statement on these issues requires further studies.

Crystalline structure

The reflection intensity of KT and its lipoidal conjugates as a function of peak position (up to 2θ=30º) is given in Fig. 3C. For lipid-containing compounds, generally, lattice parameters are obtained from small-angle reflection analysis (2θ<10º), while wide-angle reflections represent the alkyl chain arrangement.[34,35] XRD patterns of longer chain conjugates of KT (i.e., C_{16}-KT, C_{12}-KT, and C_{10}-KT) showed a highly ordered lamellar crystalline structure; which is also witnessed by thermal analysis data. C_8-KT, despite possessing a crystalline structure, did not show the same thermal behavior as other conjugates. KT demonstrated an amorphous XRD pattern.

Morphology

Through visual examination of the lyophilized compounds, two different appearances of white-colored opaque powders (C_{16}-KT, C_{12}-KT, and C_{10}-KT), and colorless hard fragile gel-like masses (C_8-KT and KT) were observed (Fig. 4A). Polarized and SEM micrographs of KT and its conjugates are represented in Fig. 4B and 4C, respectively. Under the polarized light, C_{16}-KT showed needle-like

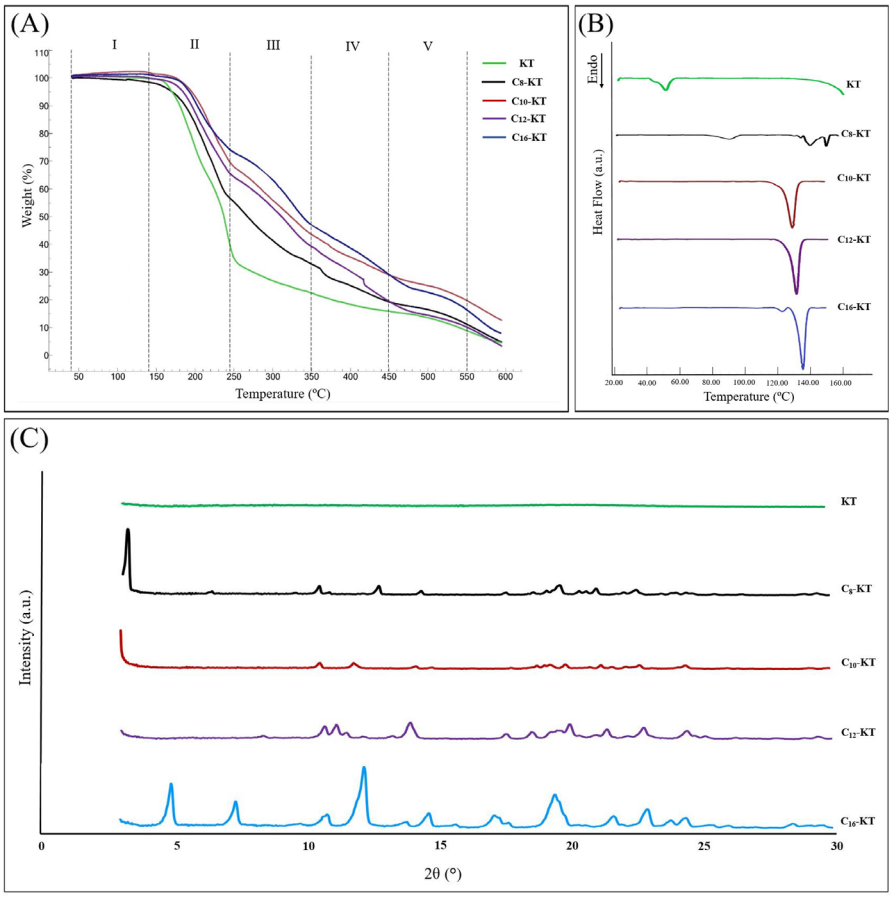

Fig. 3. (A) TGA thermograms, (B) DSC thermograms, and (C) XRD spectra of KT and its amphiphilic derivatives of caprylic acid (C8-KT), capric acid (C10-KT), lauric acid (C12-KT), and palmitic acid (C16-KT).

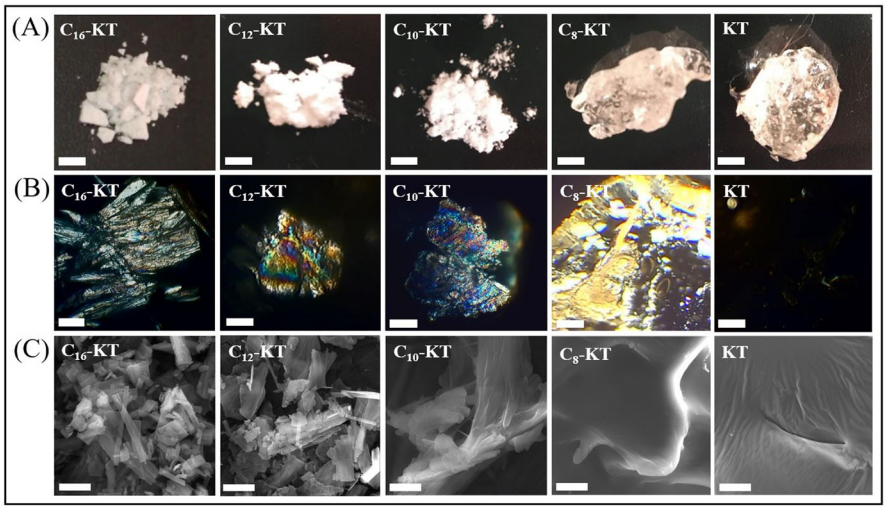

Fig. 4. Images of KT and its conjugates under (A) Visual examination (scale bar = 3 mm), (B) Polarized microscope (scale bar = 50 µm), and (C) Scanning electron microscope (SEM) (scale bar = 5 µm).

aggregates with a distinct multicolored birefringence. Such acicular morphology was also observed in the SEM image. C_{12}-KT and C_{10}-KT resembled irregular morphologies with a noticeable multicolored birefringence under the polarized light and flake-shaped particles in the SEM images. Polarized micrographs of C_8-KT exhibited yellow birefringence. The SEM images of both C_8-KT and KT displayed strikingly similar characteristics, with no signs of aggregated particles. However, it is worth nothing that KT did not show any birefringence in contrast to previous cases. All conjugates were anisotropic crystals, while KT was not visible under polarized light due to its isotropic nature (amorphous, relying on XRD).

Solubility

The predicted water solubility values of KT and its conjugates are shown in Table 2. Unlike the high solubility of the parent peptide in water (11.30×10^3 mg/L), there is a downtrend in the solubility of its lipoidal derivatives; so that the aqueous solubility of the lipoidal conjugates varies from freely soluble (C_8-KT, 191.55 mg/L) to slightly soluble (C_{16}-KT, 2.02 mg/L). Accordingly, the ability of water to dissolve our designed conjugates is advantageously higher than the commercialized peptide (P<0.001).

Surface tension and CMC

Experimental surface tension values of KT and its lipoidal conjugates at the static zone are given in Table 2. The surface tension of water (experimentally obtained 70.80±0.05 mN/m) was markedly lowered by all KT derivatives (P<0.05) which signifies the surface acting behavior of all KT derivatives at the examined concentrations. The higher the lipophilicity of the compound, the lower the concentration at which the surface tension is significantly reduced. As expected, KT did not change the surface tension of water at the studied concentrations, regarding its hydrophilic nature. In general, at low concentrations, poorly water-soluble molecules are more likely to be located at the water-air interface and lower the surface tension than hydrophilic compounds.

The corresponding CMC values recorded by the tensiometer are listed in Table 2. The results show that the carbon tail length of the conjugates is inversely proportional to the CMC value. When conjugates merely differ in the aliphatic tail length, usually there is a considerable variation in CMC values. These results correlate favorably with the previous findings; as it has been proven that in a homologous series, once the tail length as an indicator of the hydrophobic region increases, the CMC declines.[33]

Particle size

The hydrodynamic diameters of the particles composed of lipoidal conjugates in the aqueous media are given

Table 2. *In-silico* prediction of water solubility (S) of KT and its lipoidal derivatives along with the experimental surface tension and critical micelle concentration (CMC)

Compound	MW (Da)	Calculated logS	Calculated Solubility (mg/L)	Descriptive Solubility	Surface Tension (mN/m)	CMC (mg/L)
KT	247.3	-1.34	11.30×10^3	Very soluble	70.76±0.00	_
C_8-KT	373.5	-3.29	191.55	Freely soluble	47.90±0.06	194.95±0.05
C_{10}-KT	401.5	-4.01	39.24	Soluble	46.48±0.27	42.24±0.06
C_{12}-KT	429.6	-4.48	14.22	Sparingly soluble	43.35±0.36	15.31±0.05
C_{16}-KT	485.7	-5.38	2.02	Slightly soluble	47.53±0.35	1.89±0.44

Data are mean ± SD, n=3

in Table 3. A well-separated bimodal distribution was observed for all samples with a hydrodynamic radius (R_H) of 3-9 nm for the first distribution and 39-178 for the second. Such a phenomenon could be attributed to different supramolecular structures having distinct translational diffusion coefficients (D). The obtained R_H is correlated to D adopting the Stocks-Einstein law (Eq.2) for the diffusion of spherical particles through an infinite diluted liquid

$$R_H = K_B T/6\pi\eta D_0 \quad \text{(Eq.2)}$$

where K_B is the Boltzman constant (J/K), T is the absolute temperature, η is the solvent viscosity and D_0 stands for translational diffusion coefficients at infinite dilution.[36] Being extra-diluted ($D \approx D_0$), it is possible to calculate D_{fast} and D_{slow} (D_0 for the first and second peaks, respectively) for each sample (Table 3). The observed bimodal distribution pattern concurs well with what has been previously reported for other lipoidal conjugates.[37,38]

Stability

The compounds' stability ranges in the aqueous medium after 72 hours were determined as follows: KT - 99.7-100.3%, C_8-KT - 98.9-101.6%, C_{10}-KT - 96.6-103.7%, C_{12}-KT - 96.2-101.8%, and C_{16}-KT - 93.2-104.2%. To the best of our knowledge, there is no standard protocol for the determination of peptide stability in Pharmacopoeias. However, since the assay range of most pharmaceutical peptides is 90-110% in the United States Pharmacopoeia (USP), all peptides were considered chemically stable under experimental conditions.

Ex-vivo skin permeation

Skin permeation profiles of peptides along with their permeability coefficients (Kp values) and the related data are provided in Fig. 5 and Table 4. As represented, Kp values of lipoidal conjugates were significantly (P<0.001) higher than that of KT (0.003×10^{-4} cm/h) by about 1600-22000 times with the following order: C_8-KT>C_{10}-KT>C_{12}-KT>C_{16}-KT. Statistically, there were highly significant differences between Kp values of C_8-KT and other conjugates (P<0.001) as well, whereas the differences between Kp values of C_{10}-KT, C_{12}-KT, and C_{16}-KT were not significant (P>0.05).

According to Table 4, C_8-KT showed the highest permeation percentage (33.2%), which was significantly (P<0.001) higher than those of KT (0.004%) and the longer-chain lipoidal conjugates (i.e., C_{10}-KT, C_{12}-KT, and C_{16}-KT) that exhibited intermediate permeation percentages of 2.3, 0.5, and 2.6%, respectively. There were no significant differences among C_{10}-KT, C_{12}-KT, and C_{16}-KT in this regard (P>0.05). By subtracting the amount permeated through the skin and the recovered amount in the donor phase at the end of the experiment from the total initial amount applied to the skin, the trapped/unrecovered proportion of each drug was obtained (Table 4). This value is expected to be mostly the amount trapped in skin layers (intact epidermis and dermis), but it also might encompass the drug attached to the skin surface or accumulated in the appendages (such as hair follicles and hair shafts). Based on Table 4, 97.7% of KT remained in the donor phase after 48h and only about 2% was trapped. In the case of conjugates, there was a regular trend in the trapped amounts of drugs, so, the longer the fatty acid chain (the higher lipophilicity and molecular weight), the greater the amount of entrapment. Therefore, of all, C_8-KT with the lowest molecular weight, logP, and tail length showed the lowest skin accumulation (≈34%) and C_{16}-KT exhibited the highest (≈93%).

Table 3. Hydrodynamic radii (R_H) obtained from DLS along with corresponding translational diffusion coefficients for the first and second peaks (D_{fast} and D_{slow}, respectively)

Structure	First Distribution		Second Distribution	
	R_H (nm)	$D_{fast}\times10^{-11}$ (m^2/s)	R_H (nm)	$D_{slow}\times10^{-12}$ (m^2/s)
C_8-KT	9.08±2.87	2.18±0.69	178.1±24.51	1.1±0.1
C_{10}-KT	4.36±1.02	4.56±0.42	171.0±18.28	1.2±0.2
C_{12}-KT	5.62±0.80	3.55±0.72	38.80±1.49	5.1±0.3
C_{16}-KT	3.12±0.24	6.37±0.22	39.41±4.94	5.1±0.8

Data are mean ± SD, n=3

Table 4. Calculated permeation parameters including flux, permeability coefficient (Kp), and Kp ratio of peptides along with their permeation data through the rat skin from their saturated solutions (maximum thermodynamic activity) over 48 h

Peptide	Drug concentration in the donor phase* (mg/mL)	Flux (μg/cm²/h)	Kp ($\times10^{-4}$ cm/h)	Kp ratio	Permeated drug through the skin (%)	Residual drug in the donor phase (%)	Unrecovered/ trapped drug** (%)
KT	11.3	0.003±0.000	0.003±0.000	1	0.004±0.001	97.73±1.688	≈2%
C_8-KT	0.192	1.084±0.085	56.61±2.024	22059	33.24±9.562	21.29±3.851	≈34%
C_{10}-KT	0.039	0.032±0.009	9.75±1.06	3798	2.314±1.087	55.23±3.377	≈42%
C_{12}-KT	0.014	0.016±0.006	8.81±2.29	3434	0.499±0.070	21.49±7.454	≈78%
C_{16}-KT	0.002	0.001±0.000	4.22±1.26	1644	2.628±0.368	4.197±1.308	≈93%

Data are mean ± SD, n=3.

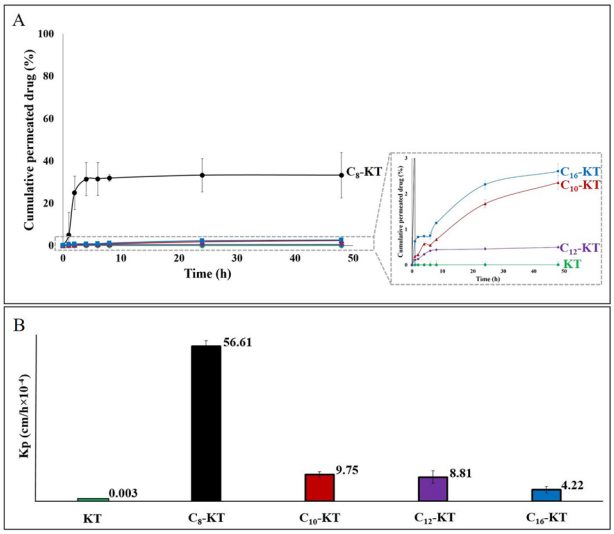

Fig. 5. (A) Permeation profiles of KT and its lipoidal conjugates through the rat skin over 48h and (B) The corresponding permeability coefficients (Kp).

Discussion

The thermal analysis of peptide conjugates showed an ordered trend based on the lengths of fatty acid attached. Moreover, compounds with similar physical appearances (i.e., KT and C_8-KT vs. C_{10}-KT, C_{12}-KT, and C_{16}-KT) showed more similarities in terms of thermal behavior, stability, decomposition profile, and melting point. According to DSC results (Fig. 3B), unlike the longer-chain conjugates, C_8-KT shows glass transition (T_g), instead of melting point (T_m). Relying on the evidence obtained, the foremost cause of this discrepancy is probably because C_8-KT is a liquid crystalline glass below its T_m (e.g., at ambient temperature); however, being exposed to higher temperatures, it transforms into a thermotropic liquid crystalline substance.[39] Nevertheless, a definitive statement is required to further evidence. In summary, the shorter the fatty acid chain length, the lower the crystallinity and melting point, and the higher the aqueous solubility of the conjugate. When the logS (mg/L) of peptides are drawn as a function of the carbon tail length, a linear relationship is achieved with a much-closed R^2 to 1. It has been previously shown that logS has a high negative relationship with the carbon number in a homologous series, wherewith our finding fits perfectly.[40] In the longer chain compounds (n=12, 16), the solubility of conjugates is higher than their corresponding fatty acids, which indicates the effect of the hydrophilic head in modulating lipophilicity. However, as the tail gets shorter (n=8, 10) this trend is reversed. The solubility of a substance is an outcome of the impact of two structural factors: hydrophobicity and crystallinity. These factors have been related quantitatively to solubility through the modified general solubility equation (GSE) (Eq.3)[41]:

$$\log S = 0.5 - 0.01(T_m - 25) - \log P \qquad \text{(Eq.3)}$$

The low aqueous solubility of hydrophobic substances is due to their restricted interaction with water (poor hydration). Hydration-limited solubility is typically prominent for high-molecular-weight lipophilic molecules. LogP of 2-3 is generally considered as the cut-off limit for hydration, above which hydration of molecule faces a serious obstacle. Solid-state-limited solubility is a completely different mechanism that leads to the same result. In this case, the strengthened crystalline lattice resists disintegration as the prerequisite of dissolution.[42] This is why the solubility of C_8 is much higher than C_8-KT (logP of 3.05 and 1.44, respectively). Despite the lower logP, C_8-KT has a partial crystallinity whereas C_8 is completely amorphous; thereby, the solid-state overweighs the hydrophobic nature. Similarly, in molecules with a 10-carbon chain, the solid-state surpasses hydrophobicity, albeit with a slight advantage. However, in longer chain substances, logP takes precedence. This effect is visually demonstrated in Fig. 6.

All synthesized conjugates reduced the surface tension of water. This ability has been also reported for other lipidated peptides. For instance, the experimental surface tension of Pal-KTTKS at its equilibrium zone has been reported to be 50.3±0.40 mN/m. Nevertheless, KTTKS did not dramatically change the surface tension of water (69.00±2.7 mN/m).[43] Additionally, NMR diffusometry has already proved the surface-active behavior of Pal-KTTKS.[44] It has been shown that a majority of self-assembling peptides possess a similar structure, composed of a peptide block and a hydrophobic alkyl chain. Being exposed to aquatic media, the presence of an alkyl tail leads to a protein-like three-dimensional structure; thus, the formation of supramolecular structures (e.g., micelles, vesicles, and nanofibers) is very likely.[45] The normal range of micelle particle size is 5-100 nm.[46] So, the hydrodynamic radii of the first peaks (<10 nm) for all samples are typical for micellar structures. Moreover, our values correlate satisfactorily with previous findings of peptide amphiphile-based micelles.[40,41] In a study,

the second peak has been attributed to the formation of liposomal structures.[40] However, due to the size overlap of small unilamellar niosomes (10-100 nm) with micelles, it is not possible to make a definite comment based on this parameter alone.[47] Regardless of the type of supramolecular architecture formed, the ability of conjugates to self-assembled in water is significant. It offers valuable insights into their potential as carrier-free systems.

According to the absorption studies, Kp values of all peptide conjugates were significantly higher than KT. Also, there was an inverse relationship between Kp values and chain lengths of the conjugates. These findings are in line with what Namjoshi et al. have previously reported on skin permeation of peptide conjugates. Accordingly, a native peptide with a high polarity showed poor permeation through the stratum corneum. In the case of conjugates, the length of the fatty acid chain (and thus, logP) affected the skin permeation as well as drug binding within the lipid-rich stratum corneum. So, the more lipophilic conjugates, the stronger partitioning into and binding to the stratum corneum.[48] Previous studies have shown that a variety of long-chain fatty acids are present in the stratum corneum.[49,50] Also, Mortazavi et al. have reported a 48% accumulation of Pal-KTTKS in the epidermis and concluded that this phenomenon is probably due to drug entrapment in the intercellular liquid crystalline structure of the stratum corneum, as a result of its structural similarity to the intercellular lipids.[16] Accordingly, long-chain conjugates of KT (with linear structures) may also be located inside the lipid bilayers, thus preventing them from passing through. The present data (Fig. 5) emphasizes the well-known parabolic relationship between percutaneous absorption and lipophilicity of the penetrants. Such behavior is due to the complex skin barrier comprising serial lipophilic (the stratum corneum) and hydrophilic (the viable epidermis and dermis) compartments. In such a system, a double function barrier exists against both hydrophilic molecules (KT in our case), which cannot easily be partitioned into the stratum corneum, and extremely lipophilic molecules (our long-chain conjugates) which trap inside the barrier. The peak is related to the optimal region of absorption (optimum lipophilicity), C_8-KT in our case. To summarize, C_8-KT with maximum skin permeation seems a promising anti-aging candidate. Besides, the Kp values of C_{10}-KT and C_{12}-KT are about the same as that of some other successful peptide conjugates which have already been reported in the literature.[16, 48] Therefore, all the designed lipoidal conjugates deserve to be given special attention as novel anti-aging candidates with improved permeation.

Conclusion

To sum up, this work presented novel lipoidal conjugates of KT (C_8-KT, C_{10}-KT, C_{12}-KT, and C_{16}-KT) as anti-aging candidates with improved physicochemical characteristics. These novel conjugates outperformed KT, in terms of amphiphilicity-related features (e.g., logP, surface acting, and self-assembling capability) which provides clues about the capability to form self-deliverable formulations and/or provide permeation enhancement effects. Besides, reducing the chain length positively affected the aqueous solubility; so that solubility of C_{12}-KT, C_{10}-KT, and C_8-KT was determined to be about 7-, 20, and 95-times higher than Pal-KT, respectively. Moreover, the crystallinity studies exhibited a less compact structure of designed conjugates than Pal-KT. According to the *ex-vivo* skin absorption studies, the maximum and minimum skin permeation were assigned to C_8-KT (33.2%) and KT (0.004%), respectively; while the longer-chain conjugates were in between. Kp values of the C_8-KT, C_{10}-KT, C_{12}-KT, and C_{16}-KT were about 22000, 3800, 3400, and 1600 times higher than that of KT, respectively. This indicates the

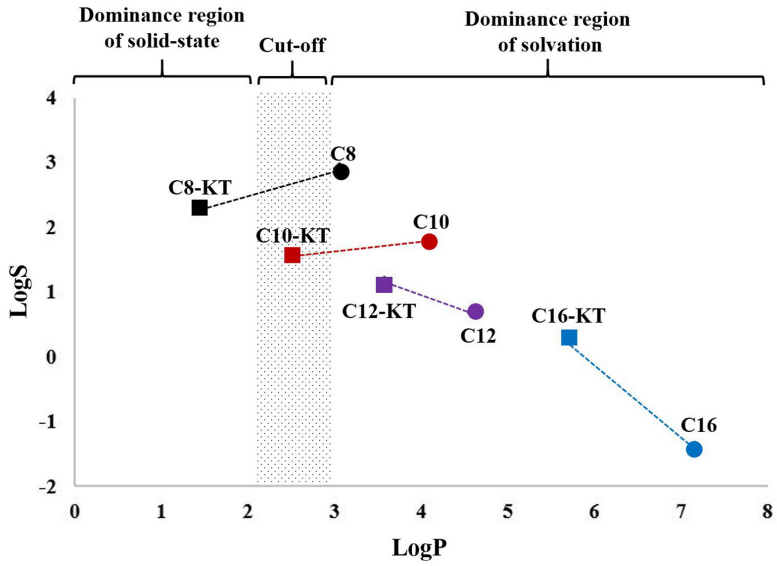

Fig. 6. Location of homologous series of KT derivatives and corresponding fatty acids by the dominance region of solvation limiting factors (to simplify the solubility changing trend, each KT derivative is connected by a dashed line to its corresponding fatty acid)

Research Highlights

What is the current knowledge?

√ Despite their efficacy, anti-wrinkle peptides (e.g., dipeptide KT) cannot permeate the skin in therapeutic amounts due to their hydrophilic nature.

√ Lipoidal conjugates solve the hydrophilicity problem; but, the increased molecular weight creates a new problem for optimized absorption.

What is new here?

√ Different short-mid chain fatty acids (C8, C10, and C12) alongside C16 (as the control) were conjugated to KT.

√ Fatty acid conjugation increased skin permeation of KT by about 1600 to 22 000 times, depending on the chain length.

√ Lipophilicity increased by chain length and the highest permeability was observed with C8-KT (lowest molecular weight, moderate logP).

√ Solubility, crystallinity, and self-assembling capability were affected by chain length.

√ C8-KT, C10-KT, and C12-KT are expected to be formulated as self-deliverable systems.

superiority of the lipoidal conjugates as skin permeants and highlights the role of chemical modification as an effective strategy to improve the skin permeation of peptides. Nevertheless, the obtained absorption data (in solution state) are not the only criteria for choosing the optimal molecule. Therefore, given the desirable performance of the lipoidal conjugates in preformulation studies as well as the acceptable Kp values, none of the conjugates were left out for further investigations. Currently, we are in the process of designing self-assembled self-deliverable topical formulations to determine if this strategy can further improve skin absorption of lipoidal conjugates. This study is anticipated to help in the development of optimized topically-applied peptide conjugates for clinically effective rejuvenating formulation using a simple but logical design.

Acknowledgments

We would like to thank Dr. S. M. Mortazavi, Dr. M. Rezaeian, and Ms. R. Ramezani for their valuable suggestions.

Author Contributions

Conceptualization: Hamid Reza Moghimi, Farzad Kobarfard.
Data curation: Mahsa Sayed Tabatabaei.
Formal analysis: Hamid Reza Moghimi, Farzad Kobarfard, Reza Aboofazeli, Mahsa Sayed Tabatabaei.
Funding acquisition: Hamid Reza Moghimi, Farzad Kobarfard, Reza Aboofazeli.
Investigation: Mahsa Sayed Tabatabaei, Sorour Ramezanpour.
Methodology: Mahsa Sayed Tabatabaei, Hamid Reza Moghimi, Farzad Kobarfard, Sorour Ramezanpour.
Project Administration: Hamid Reza Moghimi, Farzad Kobarfard.
Software: Mahsa Sayed Tabatabaei.
Supervision: Hamid Reza Moghimi, Farzad Kobarfard.
Writing-original draft: Mahsa Sayed Tabatabaei.
Writing-review & editing: Mahsa Sayed Tabatabaei, Hamid Reza Moghimi, Farzad Kobarfard.

Ethical statement

All animal experimental procedures were based on the guideline "Iran National Committee for Ethics in Biomedical Research," which has been previously approved by the ethics committee of Shahid Beheshti University of Medical Sciences (The ethical approval number: IR.SBMU.PHNM.1395.612-613).

Competing Interests

The authors declare no conflict of interest.

Funding

This study was performed within the framework of the Ph.D. thesis of M. S. Tabatabaei at the Department of Pharmaceutics and Pharmaceutical Nanotechnology, School of Pharmacy, Shahid Beheshti University of Medical Sciences (SBMU), Tehran, Iran; and was financially supported by Protein Technology Research Center, SBMU, Tehran, Iran [Grant Nos.: 10873 and 10874].

References

1. Almeida H, Matos L. Human ageing, a biological view. In: Neves D, editor. *Anti-ageing nutrients: evidence-based prevention of age-associated diseases*. Hoboken, NJ: John Wiley & Sons Inc.; **2015**.
2. Gupta MA, Gilchrest BA. Psychosocial aspects of aging skin. *Dermatol Clin* **2005**; 23: 643–8. https://doi.org/10.1016/j.det.2005.05.012
3. Neubert RHH, Sommer E, Schölzel M, Tuchscherer B, Mrestani Y, Wohlrab J. Dermal peptide delivery using enhancer moleculs and colloidal carrier systems. Part II: tetrapeptide PKEK. *Eur J Pharm Biopharm* **2018**; 124: 28-33. https://doi.org/10.1016/j.ejpb.2017.12.004
4. Sommer E, Neubert RHH, Mentel M, Tuchscherer B, Mrestani Y, Wohlrab J. Dermal peptide delivery using enhancer molecules and colloidal carrier systems. Part III: Tetrapeptide GEKG. *Eur J Pharmacol* **2018**; 124: 137-44. https://doi.org/10.1016/j.ejps.2018.08.034
5. Mortazavi SM, Moghimi HR. Skin permeability, a dismissed necessity for anti-wrinkle peptide performance. *Int J Cosmet Sci* **2022;** 44: 232-248. https://doi.org/10.1111/ics.12770
6. Abd E, Benson HA, Mohammed YH, Roberts MS, Grice JE. Permeation mechanism of caffeine and naproxen through in vitro human epidermis: effect of vehicles and penetration enhancers. *Skin Pharmacol Physiol* **2019**; 32: 132-41. https://doi.org/10.1159/000497225
7. Krishnan G, Roberts MS, Grice J, Anissimov YG, Moghimi HR, Benson HAE. Iontophoretic skin permeation of peptides: an investigation into the influence of molecular properties, iontophoretic conditions and formulation parameters. *Drug Deliv Transl Res* **2014**; 4: 222-32. https://doi.org/10.1007/s13346-013-0181-8
8. Moghimi HR, Williams AC, Barry BW. Enhancement by Terpenes of 5-Fluorouracil Permeation through the Stratum Comeum: Model Solvent Approach. *J Pharm Pharmacol* **1998**; 50: 955-64. https://doi.org/10.1111/j.2042-7158.1998.tb06909.x
9. Dhawan S, Sharma P, Nanda S. Cosmetic nanoformulations and their intended use. In: Slimani Y, S Nanda, S Rajendran, TA Nguyen, A Nanda, editors. *Nanocosmetics: Fundamentals, Applications and Toxicity*: Micro and Nano Technologies; **2020**.
10. Chaulagain B, Jain A, Tiwari A, Verma A, Jain SK. Passive delivery of protein drugs through transdermal route. *Artif Cells Nanomed Biotechnol* **2018**; 46: 472-87. https://doi.org/10.1080/21691401.2018.1430695
11. Lim SH, Sun Y, Madanagopal TT, Rosa V, Kang L. Enhanced skin permeation of anti-wrinkle peptides via molecular modification. *Sci Rep* **2018**; 8: 1-11. https://doi.org/10.1038/s41598-017-18454-z
12. Kowalczyk R, Harris PWR, Williams GM, Yang S-H, Brimble MA. Peptide Lipidation – A Synthetic Strategy to Afford Peptide Based Therapeutics. In: Sunna A, A Care, PL Bergquist, editors. *Peptides and Peptide-based Biomaterials and their Biomedical Applications*. Cham: Springer International Publishing; **2017**.

13. Ferreira MS, Magalhães MC, Sousa-Lobo JM, Almeida IF. Trending Anti-Aging Peptides. *Cosmetics* **2020**; 7: 91. https://doi.org/10.3390/cosmetics7040091
14. Lee C-M. Fifty years of research and development of cosmeceuticals: a contemporary review. *J Cosmet Dermatol* **2016**; 15: 527-39. https://doi.org/10.1111/jocd.12261
15. Palladino P, Castelletto V, Dehsorkhi A, Stetsenko D, Hamley IW. Conformation and self-association of peptide amphiphiles based on the KTTKS collagen sequence. *Langmuir* **2012**; 28: 12209-15. https://doi.org/10.1021/la302123h
16. Mortazavi SM, Kobarfard F, Manafi A, Maibach HI, Moghimi HR. Terpene conjugation: a novel approach for topical peptide delivery. *J Cosmet Sci* **2021**; 72(5).
17. Osborne R. In vitro skin structure benefits with a new antiaging peptide, Pal-KT. *J Am Acad Dermatol* **2008**; 58: AB25. https://doi.org/10.1016/j.jaad.2007.10.126
18. Tałałaj U, Uścinowicz P, Bruzgo I, Surażyński A, Zaręba I, Markowska A. The Effects of a Novel Series of KTTKS Analogues on Cytotoxicity and Proteolytic Activity. *Molecules* **2019**; 24: 3698. https://doi.org/10.3390/molecules24203698
19. Qin S-Y, Zhang A-Q, Cheng S-X, Rong L, Zhang X-Z. Drug self-delivery systems for cancer therapy. *Biomaterials* **2017**; 112: 234-47. https://doi.org/10.1016/J.BIOMATERIALS.2016.10.016
20. Imoto T, Goto M. Self-Assembled Palmitoyl-Glycine-Histidine as a Permeation Enhancer for Transdermal Delivery. *Langmuir* **2021**; 37: 8971–7. https://doi.org/10.1021/acs.langmuir.1c00889
21. N'Da DD. Prodrug strategies for enhancing the percutaneous absorption of drugs. *Molecules* **2014**; 19: 20780-807. https://doi.org/10.3390/molecules191220780
22. Potts RO, Guy RH. Predicting skin permeability. *Pharm Res* **1992**; 9: 663-9. https://doi.org/10.1023/A:1015810312465
23. Mant CT, Chen Y, Yan Z, Popa TV, Kovacs JM, Mills JB, *et al.* HPLC analysis and purification of peptides. *Peptide Characterization and Application Protocols*: Springer; **2007**. p. 3–55.
24. Tetko IV, Gasteiger J, Todeschini R, Mauri A, Livingstone D, Ertl P, *et al.* Virtual Computational Chemistry Laboratory – Design and Description. *J Comput Aided Mol Des* **2005**; 19: 453-63. https://doi.org/10.1007/s10822-005-8694-y
25. Li H, Hu D, Liang F, Huang X, Zhu Q. Influence factors on the critical micelle concentration determination using pyrene as a probe and a simple method of preparing samples. *R Soc Open Sci* **2020**; 7: 192092. https://doi.org/10.1098/rsos.192092
26. Kathe K, Kathpalia H. Film forming systems for topical and transdermal drug delivery. *Asian J Pharm Sci* **2017**; 12: 487-97. https://doi.org/10.1016/j.ajps.2017.07.004
27. Subedi RK, Oh SY, Chun M-K, Choi H-K. Recent advances in transdermal drug delivery. *Arch Pharm Res* **2010**; 33: 339–51. https://doi.org/10.1007/s12272-010-0301-7
28. Choy YB, Prausnitz MR. The rule of five for non-oral routes of drug delivery: ophthalmic, inhalation and transdermal. *Pharm Res* **2011**; 28: 943–8. https://doi.org/10.1007/s11095-010-0292-6
29. Ng KW. Penetration enhancement of topical formulations. *Pharmaceutics* **2018;** 10(2):51. https://doi.org/10.3390/pharmaceutics10020051
30. Chandrashekar NS, Rani RHS. Physicochemical and pharmacokinetic parameters in drug selection and loading for transdermal drug delivery. *Indian J Pharm Sci* **2008**; 70: 94. https://doi.org/10.4103/0250-474X.40340
31. Hussain SMS, Mahboob A, Kamal MS. Influence of lipophilic tail and linker groups on the surface and thermal properties of the synthesized dicationic surfactants for oilfield applications. *J Mol Liq* **2020**; 319: 114172. https://doi.org/10.1016/j.molliq.2020.114172
32. Knothe G, Dunn RO. A comprehensive evaluation of the melting points of fatty acids and esters determined by differential scanning calorimetry. *J Am Oil Chem Soc* **2009**; 86: 843-56. https://doi.org/10.1007/s11746-009-1423-2
33. Ryu J, Park CB. Solid-phase growth of nanostructures from amorphous peptide thin film: Effect of water activity and temperature. *Chemistry of Materials* **2008**; 20: 4284-90. https://doi.org/10.1021/cm800015p
34. McIntosh TJ. Differences in hydrocarbon chain tilt between hydrated phosphatidylethanolamine and phosphatidylcholine bilayers. A molecular packing model. *Biophys J* **1980**; 29: 237. https://doi.org/10.1016/S0006-3495(80)85128-9
35. Moghimi HR, Williams AC, Barry BW. A lamellar matrix model for stratum corneum intercellular lipids. V. Effects of terpene penetration enhancers on the structure and thermal behaviour of the matrix. *Int J Pharm* **1997**; 146: 41-54 https://doi.org/10.1016/S0378-5173(96)04766-7
36. Miller CC. The Stokes-Einstein law for diffusion in solution. *Proc R Soc Lond A Math Phys Sci* **1924**; 106: 724-49. https://doi.org/10.1098/rspa.1924.0100
37. Accardo A, Morisco A, Palladino P, Palumbo R, Tesauro D, Morelli G. Amphiphilic CCK peptides assembled in supramolecular aggregates: structural investigations and in vitro studies. *Mol Biosyst* **2011**; 7: 862-70. https://doi.org/10.1039/C0MB00238K
38. Hüttl C, Hettrich C, Miller R, Paulke B-R, Henklein P, Rawel H, *et al.* Self-assembled peptide amphiphiles function as multivalent binder with increased hemagglutinin affinity. *BMC Biotechnol* **2013**; 13: 51. https://doi.org/10.1186/1472-6750-13-51
39. Hwang JJ, Iyer SN, Li L-S, Claussen R, Harrington DA, Stupp SI. Self-assembling biomaterials: liquid crystal phases of cholesteryl oligo (L-lactic acid) and their interactions with cells. *Proc Natl Acad Sci U S A* **2002**; 99: 9662–7. https://doi.org/10.1073/pnas.152667399
40. Tolls J, van Dijk J, Verbruggen EJM, Hermens JLM, Loeprecht B, Schüürmann G. Aqueous Solubility–Molecular Size Relationships: A Mechanistic Case Study Using C_{10} - to C_{19}-Alkanes. *J Phys Chem A* **2002**; 106: 2760-5. https://doi.org/10.1021/jp011755a
41. Jain N, Yalkowsky SH. Estimation of the aqueous solubility I: application to organic nonelectrolytes. *J Pharm Sci* **2001**; 90: 234-52. https://doi.org/10.1002/1520-6017(200102)90:2<234::AID-JPS14>3.0.CO;2-V
42. Bergström CAS, Larsson P. Computational prediction of drug solubility in water-based systems: Qualitative and quantitative approaches used in the current drug discovery and development setting. *Int J Pharm* **2018**; 540: 185-93. https://doi.org/10.1016/j.ijpharm.2018.01.044
43. Mortazavi SM, Kobarfard F, Maibach HI, Moghimi HR. Effect of Palmitic Acid Conjugation on Physicochemical Properties of Peptide KTTKS: A Preformulation Study. *J Cosmet Sci* **2019**; 70: 299–312.
44. Miravet JF, Escuder B, Segarra-Maset MD, Tena-Solsona M, Hamley IW, Dehsorkhi A, *et al.* Self-assembly of a peptide amphiphile: transition from nanotape fibrils to micelles. *Soft Matter* **2013**; 9: 3558–64. https://doi.org/10.1039/C3SM27899A
45. Lee, Trinh, Yoo, Shin, Lee, Kim, *et al.* Self-Assembling peptides and their application in the treatment of diseases. *Int J Mol Sci* **2019**; 20: 5850. https://doi.org/10.3390/ijms20235850
46. Milovanovic M, Arsenijevic A, Milovanovic J, Kanjevac T, Arsenijevic N. Nanoparticles in antiviral therapy. *Antimicrobial nanoarchitectonics*. Elsevier; **2017**. p. 383-410.
47. Ag Seleci D, Seleci M, Walter J-G, Stahl F, Scheper T. Niosomes as nanoparticular drug carriers: fundamentals and recent applications. *J Nanomater* **2016**; 2016: 7372306 . https://doi.org/10.1155/2016/7372306
48. Namjoshi S, Toth I, Blanchfield JT, Trotter N, Mancera RL, Benson HAE. Enhanced transdermal peptide delivery and stability by lipid conjugation: epidermal permeation, stereoselectivity and mechanistic insights. *Pharm Res* **2014**; 31: 3304–12. https://doi.org/10.1007/s11095-014-1420-5
49. Moghimi HR, Williams AC, Barry BW. A lamellar matrix model for stratum corneum intercellular lipids. I. Characterisation and comparison with stratum corneum inter-cellular structure. *Int J Pharm* **1996**; 131: 103–15. https://doi.org/10.1016/0378-5173(95)04306-3
50. Ananthapadmanabhan KP, Mukherjee S, Chandar P. Stratum corneum fatty acids: their critical role in preserving barrier integrity during cleansing. *Int J Cosmet Sci* **2013**; 35: 337–45. https://doi.org/10.1111/ics.12042